Coherent anti-Stokes Raman scattering microscopy of human smooth muscle cells in bioengineered tissue scaffolds

Christian Brackmann,[a] Maricris Esguerra,[b] Daniel Olausson,[b] Dick Delbro,[b] Alexandra Krettek,[c] Paul Gatenholm,[d] and Annika Enejder[a]

[a]Chalmers University of Technology, Molecular Microscopy, Department of Chemical and Biological Engineering, SE-412 96 Göteborg, Sweden
[b]Sahlgrenska Academy at University of Gothenburg, Institute of Clinical Sciences, Department of Surgery, SE-413 45 Göteborg, Sweden
[c]Sahlgrenska Academy at University of Gothenburg, Institute of Medicine, Department of Internal Medicine, SE-405 30 Göteborg, Sweden
[d]Chalmers University of Technology, Polymer Science, Department of Chemical and Biological Engineering, SE-412 96 Göteborg, Sweden

Abstract. The integration of living, human smooth muscle cells in biosynthesized cellulose scaffolds was monitored by nonlinear microscopy toward contractile artificial blood vessels. Combined coherent anti-Stokes Raman scattering (CARS) and second harmonic generation (SHG) microscopy was applied for studies of the cell interaction with the biopolymer network. CARS microscopy probing CH_2-groups at $2845 \ cm^{-1}$ permitted three-dimensional imaging of the cells with high contrast for lipid-rich intracellular structures. SHG microscopy visualized the fibers of the cellulose scaffold, together with a small signal obtained from the cytoplasmic myosin of the muscle cells. From the overlay images we conclude a close interaction between cells and cellulose fibers. We followed the cell migration into the three-dimensional structure, illustrating that while the cells submerge into the scaffold they extrude filopodia on top of the surface. A comparison between compact and porous scaffolds reveals a migration depth of $<10 \ \mu m$ for the former, whereas the porous type shows cells further submerged into the cellulose. Thus, the scaffold architecture determines the degree of cell integration. We conclude that the unique ability of nonlinear microscopy to visualize the three-dimensional composition of living, soft matter makes it an ideal instrument within tissue engineering. © *2011 Society of Photo-Optical Instrumentation Engineers (SPIE)*. [DOI: 10.1117/1.3534782]

Keywords: coherent anti-Stokes Raman scattering; second harmonic generation; microscopy; smooth muscle cells; cellulose; tissue engineering scaffolds.

Paper 10307SSR received Jun. 13, 2010; revised manuscript received Dec. 3, 2010; accepted for publication Dec. 15, 2010; published online Feb. 4, 2011.

1 Introduction

An increasing demand for tissue implants to sustain a healthy and active life for an aging population makes the development of alternatives to transplanted autologous tissue of high interest. This has promoted the development of advanced polymeric biomaterials with properties comparable to those of native tissue and structure favorable for cell integration, for example cellulose synthesized by bacteria of the strain *Acetobacter xylinum* is emerging as an attractive alternative.[1,2] The random network of nanofibrils forms a hydrogel, which despite its exceptionally high water content (98%) possesses high mechanical strength,[3] making it a favorable material for scaffold applications. It also shows good biocompatibility[4] with low protein adsorption[5] and high permeability for liquids and gases. Cultivation can be made in the presence of molds and porogens of different sizes and shapes, in order to design desirable scaffold geometries at micro- and macro scales.[3,6] Successful results have been reported for its use as urethra-, trachea-, and digestive tract substitutes, as well as meniscus, bone, and skin graft materials.[1]

Of increasing interest is the development of tubular cellulose scaffolds for its use as artificial blood vessels.[3,7] Cardiovascular diseases form a world-wide health problem and have become the number one cause of death globally.[8] Only in the United States, ~500,000 coronary-artery[9] and ~1,000,000 peripheral-vascular bypass procedures are performed annually.[10] The current standard is to use the saphenous vein or the internal mammary artery as grafts.[11,12] However, one-third of the patients lack useable autologous transplants due to inadequate size or quality.[13] In addition, patients frequently need multiple-segment grafts or repeated surgery. Thus, there is an urgent need for artificial vascular implants. Advanced efforts are made to supplement the scaffold matrix with cells to obtain a fully functional graft. To facilitate the blood flow through the vessel and reduce the risk for thrombosis, tubular cellulose scaffolds are augmented with a luminal layer of endothelial cells.[14] Further functionalization of the cellulose vessels includes seeding them with smooth muscle cells (SMCs),[15] which can be stimulated to pulsatile dilatations and contractions of the vessel, further facilitating blood flow with reduced risk of clot formation. In addition, SMCs synthesize large amounts of extracellular matrix components, such as collagen

Address all correspondence to: Annika Enejder, Chalmers University of Technology, Department of Chemical and Biological Engineering, Kemivägen 10, Göteborg, 412 96, Sweden. Tel: +46-31-772-3852; Fax: +46-31-772-3801; E-mail: enejder@chalmers.se.

and elastin, promoting long-term adaptation of the vascular implant to varying physiological conditions such as exercise and vascular injuries[16] with the hope for life-lasting use of the implant.

The ability of SMCs to adhere to and proliferate on a synthetic scaffold is dependent on the chemical composition of the material used as well as its structure.[6, 17–20] To improve our understanding for how the material properties affect cell integration and proliferation, reliable methods to characterize the morphology of the scaffold matrix and its interaction with living cells are needed. Different microscopy techniques are, for this purpose, used within tissue engineering such as fluorescence microscopy, electron microscopy, and atomic force microscopy. Unfortunately, all are associated with severe limitations, preventing studies of soft, wet materials such as cellulose.[21–24] In many situations only the most superficial sample layer can be probed, providing information of merely topographical character without access to the full three-dimensional morphology below the surface. In addition, the many sample preparation procedures such as labeling, fixation, dehydration, freeze-drying, and material coating, potentially affect both sample structure and composition; hence the sample is studied in a modified state. Many of these limitations are avoided by applying any of the increasingly used nonlinear microscopy techniques, which allow for minimally-invasive, high-resolution, three-dimensional imaging of soft, organic materials and living cells. The spatial resolution of nonlinear techniques (typically 300 nm laterally and 1 μm axially) together with the ability to probe deep into samples make these methods clearly suitable for characterization of tissue engineering constructs often consisting of nano- to micrometer-sized structures arranged in thicker three-dimensional matrices.

Nonlinear microscopy techniques such as second harmonic generation (SHG) and two-photon fluorescence (TPF) have successfully been applied for imaging of scaffold structure, extracellular matrix components, and cells in tissue engineering.[21] With this work we show the strength of yet another nonlinear microscopy technique for tissue engineering applications, coherent anti-Stokes Raman scattering (CARS) microscopy, probing vibrations of molecular bonds for image contrast. The high vibrational Raman cross sections of many hydrogen-carbon bonds make the technique suitable for imaging of polymers[25, 26] and in particular lipids, the latter by probing CH_2 groups in the lipid acyl chains.[27, 28] Tissue engineering constructs in many cases consist of a polymer scaffold material seeded with cells for further growth and regeneration. CARS microscopy has the ability to selectively visualize the polymer scaffold but also cell arrangements by probing lipid-rich structures and membranes, making it a useful instrument within tissue engineering. Moreover, the combination of CARS microscopy with other nonlinear methods, such as SHG and TPF, permits simultaneous imaging of multiple sample structures and hence their interaction; the scaffold modules, the cells, and native extracellular matrix components such as collagens.

In the present work, this capability is exemplified with studies on the integration of human SMCs in cellulose scaffolds using combined CARS and SHG microscopy. The morphology of the scaffold and its impact on the proliferation of SMCs is monitored at sub-micrometer resolution and in full three dimensions. Whereas CARS microscopy visualizes the arrangement of the cells in the scaffold, the repetitively ordered molecular arrangement of the cellulose fibers makes it possible to visualize them with SHG microscopy.[23, 29] Thus, by combining the two microscopy modalities, the interaction between cells and cellulose fibers can be assessed in detail and the full scenario of cell integration, proliferation, and differentiation can be followed in the cellulose matrix to obtain detailed knowledge on these for tissue engineering important processes.

2 Materials and Methods

2.1 Smooth Muscle Cell Isolation and Culture

Human smooth muscle cells were isolated from saphenous veins available as excess material from bypass surgery with two anonymous donors; hence no ethical permission was required. Cells were isolated from the tunica media by explant technique. Briefly, the media was separated from the intima and adventitia, the tissue was cut into 1–2 mm^2 pieces and placed in six-well polystyrene tissue culture plates. Tissue pieces were covered with cover slips and the wells filled with 2 mL Dulbecco´s Modified Eagle Medium supplemented with 20% fetal calf serum (FCS), penicillin/streptomycin (5U/mL), Na-pyruvate (1 mM), nonessential amino acids (0.1 mM) and L-glutamine (2 mM, Invitrogen, Paisly, UK). Medium, supplements, and solutions were obtained from PAA (Linz, Austria), if not otherwise specified. Cells were grown in humidified incubators at 37°C and with 5% CO_2. At confluence, cells were detached with trypsin/EDTA and expanded. Further culturing after the first passage was done in medium containing 10% FCS and the same amount of supplements as before. SMCs were identified by morphological appearance as well as by positive immunostaining and detection of smooth muscle α-actin (SM α-actin). All cultures were negative for mycoplasma.

2.2 Preparation of Cellulose Scaffolds with SMCs

The cellulose production followed the concept of Bodin et al.[3] Briefly, cellulose was produced by *Acetobacter xylinum* fermentation, forming scaffolds of tubular geometry using a configuration with a silicon tube immersed into the culture. A flow of pure oxygen was running through the semi-permeable silicon tube and cellulose was produced at the interface between the bacterial suspension and the tube, where the bacteria have access to oxygen. After a growth period of seven days, the cellulose tubes were purified by alkali treatment, repeatedly washed, and finally autoclaved. Circular subsamples, 0.8 mm in diameter, of cellulose were punched out and placed on microplates, giving access to either the compact, luminal side of the tubular scaffold or the porous, external side. This enabled investigations on the impact of scaffold morphology on the cell integration. The cellulose samples were seeded with cultures of SMCs proceed until passage 4–5 at a density of 10 000 cells per cm^2. Cells were subsequently cultured for three and eight days at which time points the specimens were analyzed by CARS and SHG microscopy, requiring no sample preparation. An overview of the logistics of the experiments is given in Fig. 1.
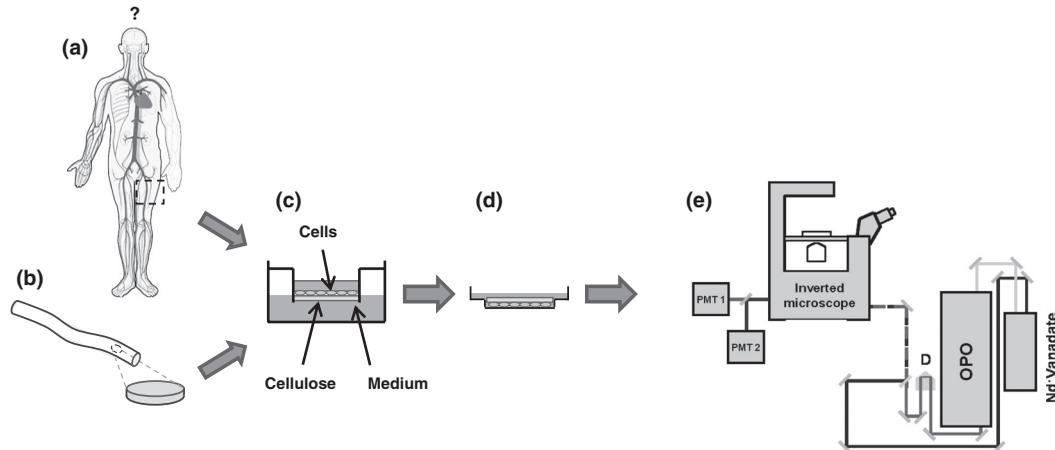
Fig. 1 Outline of the experiments. (a) Smooth muscle cells originating from saphenous veins of anonymous patients were harvested, cultured, and seeded on (b) biosynthesized tubular cellulose scaffolds. (c) After further cultivation and growth on tissue culture plates the seeded scaffold was (d) mounted for investigation of cell-scaffold integration by means of (e) combined CARS and SHG microscopy. The major components of the experimental setup are a Nd:Vanadate pump laser, an optical parametrical oscillator (OPO), an inverted microscope, and a single-photon counting photomultiplier tubes (PMTs). The 1064 nm beam from the pump laser is combined with the OPO output using dichroic mirrors prior to entering the microscope. Temporal overlap between laser pulses is achieved using a delay line (D). For further details see Sec. 2.

2.3 Nonlinear Microscopy

The setup for nonlinear microscopy [see schematic in Fig. 1(e)] consists of a pulsed, near-infrared laser system combined with an inverted Nikon Eclipse TE2000-E microscope, equipped with a Nikon C1 scanning head. The laser system consists of a high-power Nd:Vanadate laser (HighQ Laser Production GmbH, IC-LASER-10000-ps), pumping an optical parametric oscillator (APE GmbH, Levante Emerald OPO). The pump laser emits pulses with duration of 7–8 ps at a repetition rate of 76 MHz. The output power is split between the fundamental wavelength 1064 nm and the second-harmonic at 532 nm with typical average powers of 500 mW and 4W, respectively. The 532 nm beam is used to pump the Emerald OPO, which generates tunable wavelengths in ranges 690–990 nm (signal beam) and 1150–2300 nm (idler beam). The inherently synchronized OPO and 1064 nm beams are combined using dichroic mirrors and coupled into the microscope through the scanning unit. Temporal overlap of the pulses at the sample is achieved by use of a variable delay line [marked D in Fig. 1(e)] in the OPO beam path. The 1064 nm beam serves as the Stokes beam in the CARS process and the output from the OPO tuned to 817 nm as the pump/probe beam for excitation of the symmetric stretch vibration of CH_2 groups at 2845 cm^{-1}. In addition to the CARS signal generation, the OPO beam induces the SHG process in the sample. The beams illuminate the sample from below (inverted microscope) and are focused using an oil immersion objective (40× Nikon Plan Fluor N.A. 1.3). Typical average laser powers at the sample position are 40 mW for the 817 nm beam and 20 mW for the 1064 nm beam.

The generated signals can either be collected with a lens mounted in the forward, transmission direction or by the objective in epi-mode (back-reflected). All data presented in this work were collected in epi-direction and the signals were registered by single-photon counting photomultiplier tubes (Hamamatsu PMC 100–1 for SHG and Hamamatsu PMC 100–20 for CARS). A dichroic beam splitter separates the 409 nm SHG signal and the 663 nm CARS signal to enable simultaneous detection using two different detectors. Band-pass filters (2 Chroma HQ400/40 for SHG and 2 Chroma HQ665/65 + 2 Chroma HQ650/50 for CARS) are used to isolate the signals by efficient suppression of scattered excitation light.

Two-dimensional microscopy images are recorded point-wise by scanning the laser beams over the sample and three-dimensional imaging (z-stacks) is achieved by vertical translation of the objective for measurements in different horizontal planes.

For microscopy measurements cellulose scaffolds seeded with SMCs were placed in Petri dishes with a 0.17 mm thick glass bottom (Fig. 1). A small volume of medium was added to the sample to prevent drying. Visual information on the arrangement of cellulose fibers and SMCs was acquired as single images as well as z-stacks with fields of view ranging from 40×40 to 200×200 μm. Image acquisition times were 20 or 60 seconds per image.

3 Results and Discussion

3.1 Nonlinear Microscopy of Human Smooth Muscle Cells and Cellulose Scaffold

Figure 2(a) shows an ensemble of SMCs established on a cellulose scaffold of compact architecture after eight days of growth visualized by means of conventional differential interference contrast (DIC) microscopy. The cell shapes and inner structures can be clearly distinguished, whereas the cellulose fibers are invisible. As a consequence, the image lacks information on the actual contact and interaction between SMCs and the supporting cellulose scaffold. However, this information can be obtained from the nonlinear microscopy images shown in Figs. 2(b)–2(e), where the fibrillar cellulose material and cells are visualized by means of SHG and CARS microscopy, respectively. The fibrous structure of the cellulose surrounding the SMCs is visualized by SHG microscopy in Fig. 2(b) and the two SMCs grown on the cellulose are shown by CARS microscopy in Fig. 2(c).
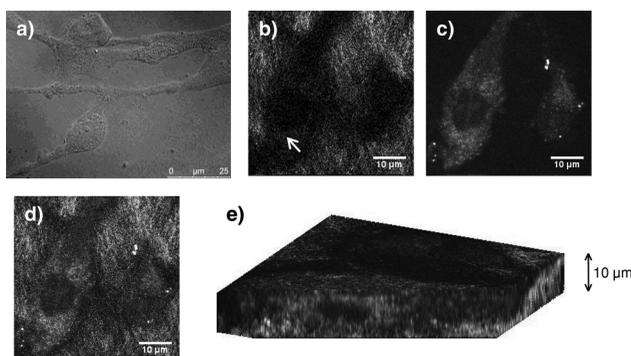
Fig. 2 SMC grown on a cellulose scaffold. (a) DIC microscopy image showing elongated cells with extended filopodia. (b) SHG microscopy image covering the same field of view visualizing the cellulose fiber matrix (blue), note the weak SHG signal also emitted from the SMC (arrow). (c) CARS microscopy image of SMCs (yellow) visualized by probing the 2845 cm^{-1} vibration of acyl CH$_2$ groups. (d) Overlay CARS (yellow) and SHG (blue) image illustrating the tight interaction between cells and the cellulose matrix. (e) 3D rendering of CARS and SHG images showing cells immersed ~10 μm into the cellulose.

Both cells are elongated and the nucleus in the left cell appears as a darker central region. Small intracellular structures generate high CARS signal at 2845 cm^{-1}, which is characteristic for lipid-rich organelles. Intracellular lipid deposits as well as micrometer-sized, membrane-rich bodies, possibly representing autophagic vacuoles have been identified in SMCs using electron microscopy[30] and both of these structures could give high CARS signals. By comparing the CARS and SHG images, it can be observed that SMCs also generate a weak SHG signal in the SHG image. This is in agreement with the composition of SMCs, containing the SHG-generating structural protein myosin.[31] In contrast to skeletal muscle tissue, the arrangement is less ordered without the striation pattern, therefore generating a low SHG signal. The overlay image and the three-dimensional rendering shown in Figs. 2(d) and 2(e) both show that the cells are immersed into the cellulose matrix. The optical sectioning capabilities of nonlinear microscopy gives valuable three-dimensional information as shown in Fig. 2(e), from which the migration depth can be determined to approximately 10 μm after eight days of growth on a compact cellulose matrix.

The combination of CARS and SHG microscopy permits detailed visualization of the contact between cells and scaffold as exemplified by the images of Fig. 3. The close-up in Fig. 3(a) shows cellular filopodia interspersed between the cellulose fibers. This signifies that a natural and close interaction has been formed between the SMCs and the cellulose fibers, as the launch of filopodia requires that adhesion points on the biopolymer surface have been established. Filopodia are also visualized in Fig. 4, where a three-dimensional rendering shows that they extend on top of the cellulose matrix [Fig. 4(b), indicated by row of arrows] while the majority of the SMC is submerged [Fig. 4(b), single arrow]. In addition, the upper-most cellulose layer [Fig. 4(a)] here exhibits an irregular wavelike pattern that differs from the more homogeneous arrangement seen in deeper layers of the stack, Fig. 4(c). One possible explanation for this pattern could be that the proliferation of filopodia induces local mechanical stresses in the cellulose, causing rearrangement of the material. Scaffold material contractions due to
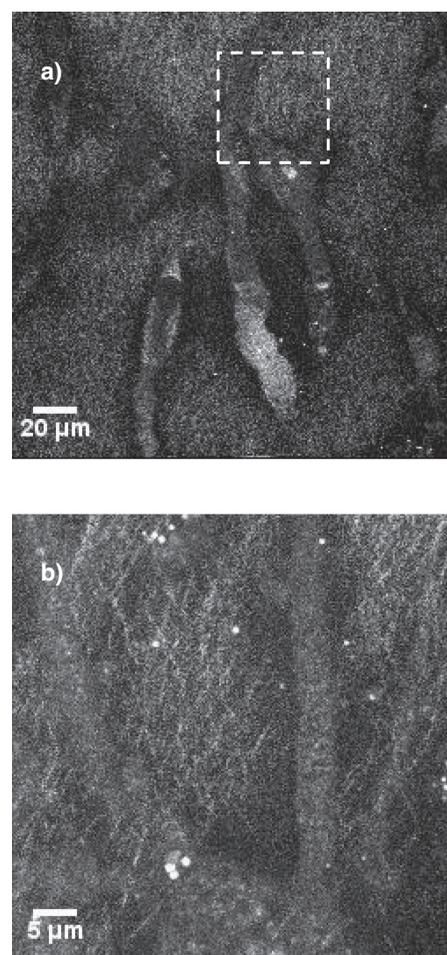
Fig. 3 Overlay CARS (yellow) and SHG (blue) microscopy images of SMCs grown on a cellulose scaffold. The close-up image in (b) shows extending filopodia interspersed in the cellulose fiber network.

growth of SMCs have been reported for polyglycolic acid (PGA) scaffolds seeded with SMCs after three weeks of growth.[17]

The applied excitation power is an important parameter when using nonlinear microscopy for characterization of samples as presented in this paper and merits some further discussion. The combined CARS and SHG measurements were carried out using picosecond excitation. Fu et al.[32] have investigated sample damage mechanisms during picosecond CARS microscopy on a carcinoma cell line and observed no photo-induced damage using a total peak power at the sample of 120 W and an intensity of approximately 0.2 TW/cm^2. In addition, they investigated dense spinal tissue, for which a peak power of 450 W did not induce sample damage. In our experiments the peak power was 110 W, corresponding to an intensity of 0.1 TW/cm^2, i.e., similar to the lower values in their study. This, together with the fact that no signs of sample damage were observed in our images, assures that the powers used were safe. For more sensitive samples excitation with femtosecond pulses could be an option, allowing for lower average powers. Femtosecond excitation is favorable for SHG microscopy, confirmed by a comparison with picosecond excitation illustrating that similar signal-to-noise ratio and image quality is obtained at 60 times lower average power.[33] However, for CARS microscopy, femtosecond
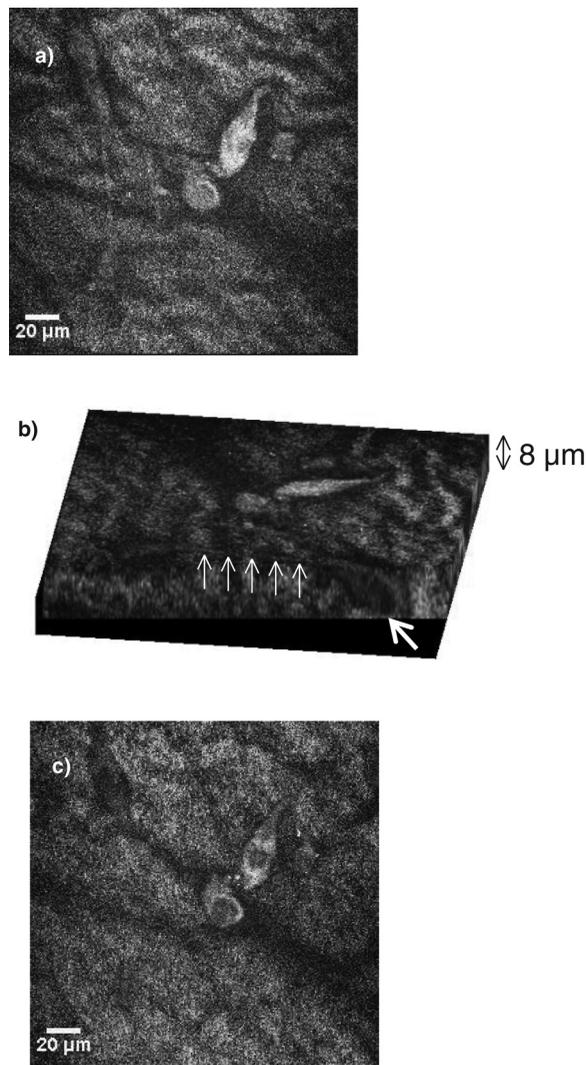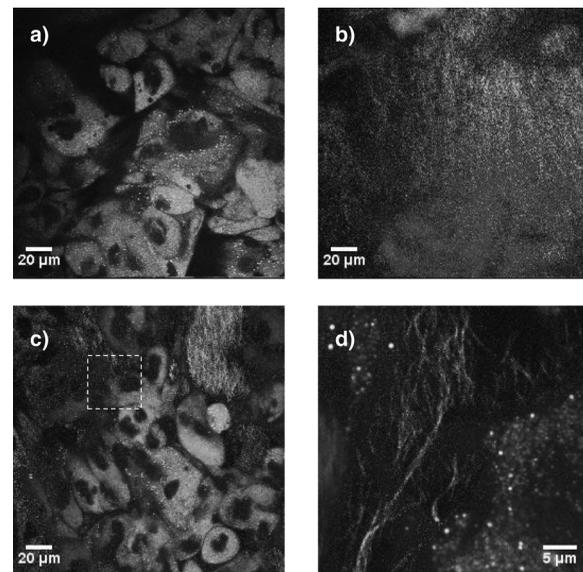
Fig. 4 Overlay CARS (yellow) and SHG (blue) images showing a network of SMCs on a cellulose scaffold. (a) A thin filipodium can be seen connecting the two cells in the left part of the image. (b) 3D rendering showing cells immersed into the cellulose with the filopodium located on top of the scaffold surface. The SHG signal (blue) shows a wavy structure in the plane of the filopodia [(a)], whereas further down in the scaffold the structure becomes more homogeneous [(c)]. This observation can be explained by mechanical stress induced in the scaffold by the formation and migration of the filopodia.

excitation is less suitable since it provides significantly lower contrast due to the broad spectral line-profile of femtosecond pulses, resulting in increased excitation of the nonresonant background signal. This drawback of femtosecond CARS has been thoroughly analyzed[34] and experimentally demonstrated.[33] Thus, for simultaneous CARS and SHG microscopy, picosecond excitation is preferably applied, restricting the excitation powers and intensities to values indicated by Fu et al.[32]

3.2 Influence of Scaffold Morphology on Cell Migration

Figure 5 shows CARS and SHG overlay images measured on SMCs grown on cellulose scaffolds of different architecture for three days; compact [Figs. 5(a) and 5(b)] and porous [Figs. 5(c) and 5(d)]. In contrast to the eight-day samples in Figs. 2–4, we

Fig. 5 CARS (yellow) and SHG (blue) overlay images of SMCs growing on compact [(a) and (b)] and porous [(c) and (d)] cellulose scaffolds. (a) Image of SMCs established on top of the compact cellulose matrix, showing a dense layer of cells and no SHG signal from cellulose fibers. When focusing ∼20 μm below the cells, a first indication of SHG signal (blue) from the cellulose fibers is observed, see (b). This indicates a limited integration of the cells into the compact cellulose matrix. A porous scaffold facilitates cell migration and the cellulose matrix can be seen in the upper-most plane together with the SMCs, as exemplified in (c). The close-up image in (d) shows individual cellulose fibers, seemingly attached to the SMC membrane.

note that the cells exhibit a rounded shape and have not adopted the elongated shape characteristic of developed SMCs.[35] This could explain, in general, the higher cell densities observed in the three-day samples compared to the eight-day samples, as the lateral cell migration has not yet been able to take place. However, the difference in local cell densities may also be attributed to seeding conditions.

The images of the compact scaffold in Figs. 5(a) and 5(b) are measured at the same lateral position in the sample but at different depths separated by 20 μm. It illustrates that a confluent multiple-cell layer [Fig. 5(a)] is already formed after three days' growth on top of the compact cellulose scaffold, here found ∼20 μm below the cells [Fig. 5(b)]. Repeated measurements at different positions confirmed a limited integration into the compact cellulose matrix. Figures 5(c) and 5(d) were measured on the surface of porous, outer side of cellulose scaffold showing cells as well as cellulose. Thus, the cells have been able to migrate into the porous cellulose matrix, again already after three days' growth. The close-up image in Fig. 5(d) clearly visualizes the intimate contact established between the SMCs and individual cellulose fibers. For both types of scaffold architectures the cells are arranged in clusters with multiple layers and their growth appears to be constricted by the surrounding cellulose matrix and neighboring cells. In agreement with our observations, studies of SMCs grown on cellulose scaffolds using electron microscopy showed a cell migration of 5–10 μm for the compact material, whereas an integration of up to 40 μm could be observed for the porous type.[15]

4 Conclusions

CARS and SHG microscopy reveals a tight interaction between SMCs and cellulose fibers, in agreement with the good biocompatibility observed for biosynthesized cellulose scaffolds. The degree of cell integration as observed in the three-dimensional images is to a large extent dependent on the architecture of the cellulose matrix, which can be designed to achieve a distribution of cells desirable for the functionality of the scaffold. Further systematic investigations of the impact of the hierarchical structure of the cellulose material on the cell integration and proliferation are required to fully characterize this relationship. This work takes full advantage of the abilities of nonlinear microscopy to provide three-dimensional, sub-micrometer resolution images of the structural and chemical composition of soft matter, enabling unique insights in the cell — scaffold interaction mechanisms of strong interest for tissue engineering applications. Thus, nonlinear microscopy has a strong potential to become an important instrument within the field of Tissue Engineering.

References

1. W. K. Czaja, D. J. Young, M. Kawecki, and R. M. Brown, "The future prospects of microbial cellulose in biomedical applications," *Biomacromolecules* **8**(1), 1–12 (2007).
2. D. Klemm, B. Heublein, H. P. Fink, and A. Bohn, "Cellulose: fascinating biopolymer and sustainable raw material," *Angew. Chem., Int. Ed.* **44**(22), 3358–3393 (2005).
3. A. Bodin, H. Bäckdahl, H. Fink, L. Gustafsson, B. Risberg, and P. Gatenholm, "Influence of cultivation conditions on mechanical and morphological properties of bacterial cellulose tubes," *Biotechnol. Bioeng.* **97**(2), 425–434 (2007).
4. G. Helenius, H. Backdahl, A. Bodin, U. Nannmark, P. Gatenholm, and B. Risberg, "In vivo biocompatibility of bacterial cellulose," *J. Biomed. Mater. Res. Part A* **76A**(2), 431–438 (2006).
5. K. Watanabe, Y. Eto, S. Takano, S. Nakamori, H. Shibai, and S. Yamanaka, "A new bacterial cellulose substrate for mammalian cell culture," *Cytotechnology* **13**(2), 107–114 (1993).
6. H. Bäckdahl, M. Esguerra, D. Delbro, B. Risberg, and P. Gatenholm, "Engineering microporosity in bacterial cellulose scaffolds," *J. Tissue Eng. Regener. Med.* **2**(6), 320–330 (2008).
7. D. Klemm, D. Schumann, U. Udhardt, and S. Marsch, "Bacterial synthesized cellulose – artificial blood vessels for microsurgery," *Prog. Polym. Sci.* **26**(9), 1561–1603 (2001).
8. "Cardiovascular Diseases," World Health Organization Fact Sheet 317 (2007).
9. "Heart Disease and Stroke Statistics – 2008 Update," American Heart Association (2008).
10. T. J. Wilt, "Current strategies in the diagnosis and management of lower-extremity peripheral vascular disease," *J. Gen. Intern. Med.* **7**(1), 87–101 (1992).
11. A. Cameron, K. B. Davis, G. Green, and H. V. Schaff, "Coronary bypass surgery with internal-thoracic-artery grafts – effects on survival over a 15-year period," *N. Engl. J. Med.* **334**(4), 216–219 (1996).
12. L. M. Taylor, J. M. Edwards, and J. M. Porter, "Present status of reversed vein bypass-grafting – 5-year results of a modern series," in *43rd Annual Meeting of the Soc for Vascular Surgery*, pp. 193–206, New York, NY (1989).
13. F. J. Veith, C. M. Moss, S. Sprayregen, and C. Montefusco, "Preoperative saphenous venography in arterial reconstructive surgery of the lower-extremity," *Surgery* **85**(3), 253–256 (1979).
14. A. Bodin, L. Ahrenstedt, H. Fink, H. Brumer, B. Risberg, and P. Gatenholm, "Modification of nanocellulose with a xyloglucan-RGD conjugate enhances adhesion and proliferation of endothelial cells: implications for tissue engineering," *Biomacromolecules* **8**(12), 3697–3704 (2007).
15. H. Bäckdahl, G. Helenius, A. Bodin, U. Nannmark, B. R. Johansson, B. Risberg, and P. Gatenholm, "Mechanical properties of bacterial cellulose and interactions with smooth muscle cells," *Biomaterials* **27**(9), 2141–2149 (2006).
16. G. K. Owens, M. S. Kumar, and B. R. Wamhoff, "Molecular regulation of vascular smooth muscle cell differentiation in development and disease," *Physiol. Rev.* **84**(3), 767–801 (2004).
17. B.-S. Kim and D. J. Mooney, "Engineering smooth muscle tissue with a predefined structure," *J. Biomed. Mater. Res.* **41**(2), 322–332 (1998).
18. B.-S. Kim, J. Nikolovski, J. Bonadio, E. Smiley, and D. J. Mooney, "Engineered smooth muscle tissues: regulating cell phenotype with the scaffold," *Exp. Cell Res.* **251**(2), 318–328 (1999).
19. L. D. Harris, B.-S. Kim, and D. J. Mooney, "Open pore biodegradable matrices formed with gas foaming," *J. Biomed. Mater. Res.* **42**(3), 396–402 (1998).
20. J. Nikolovski and D. J. Mooney, "Smooth muscle cell adhesion to tissue engineering scaffolds," *Biomaterials* **21**(20), 2025–2032 (2000).
21. I. Georgakoudi, W. L. Rice, M. Hronik-Tupaj, and D. L. Kaplan, "Optical spectroscopy and imaging for the noninvasive evaluation of engineered tissues," *Tissue Eng.* **14**(4), 321–340 (2008).
22. W. Czaja, D. Romanovicz, and R. M. Brown, "Structural investigations of microbial cellulose produced in stationary and agitated culture," *Cellulose* **11**(3–4), 403–411 (2004).
23. C. Brackmann, A. Bodin, M. Åkeson, P. Gatenholm and, A. Enejder, "Visualization of the cellulose biosynthesis and cell integration into cellulose scaffolds," *Biomacromolecules* **11**(3), 542–548 (2010).
24. Z. F. Shao, J. Mou, D. M. Czajkowsky, J. Yang, and J. Y. Yuan, "Biological atomic force microscopy: what is achieved and what is needed," *Adv. Phys.* **45**(1), 1–86 (1996).
25. T. W. Kee and M. T. Cicerone, "Simple approach to one-laser, broadband coherent anti-Stokes Raman scattering microscopy," *Opt. Lett.* **29**(23), 2701–2703 (2004).
26. E. N. Kang, H. F. Wang, I. K. Kwon, J. Robinson, K. Park, and J. X. Cheng, "In situ visualization of paclitaxel distribution and release by coherent anti-Stokes Raman scattering microscopy," *Anal. Chem.* **78**(23), 8036–8043 (2006).
27. M. Muller and A. Zumbusch, "Coherent anti-Stokes Raman scattering microscopy," *ChemPhysChem* **8**(15), 2157–2170 (2007).
28. A. Enejder, C. Brackmann, and F. Svedberg, "Coherent Anti-Stokes Raman Scattering Microscopy of Cellular Lipid Storage," *IEEE J. Sel. Top. Quantum Electron.* **16**(3), 506–515 (2010).
29. R. M. Brown, A. C. Millard, and P. J. Campagnola, "Macromolecular structure of cellulose studied by second-harmonic generation imaging microscopy," *Opt. Lett.* **28**(22), 2207–2209 (2003).
30. R. Ross, "The smooth muscle cell. II. Growth of smooth muscle in culture and formation of elastic fibers," *J. Cell Biol.* **50**(1), 172–186 (1971).
31. S. V. Plotnikov, A. C. Millard, P. J. Campagnola, and W. A. Mohler, "Characterization of the myosin-based source for second-harmonic generation from muscle sarcomeres," *Biophys. J.* **90**(2), 693–703 (2006).
32. Y. Fu, H. F. Wang, R. Y. Shi, and J. X. Cheng, "Characterization of photodamage in coherent anti-Stokes Raman scattering microscopy," *Opt. Express* **14**(9), 3942–3951 (2006).
33. F. Svedberg, C. Brackmann, T. Hellerer, and A. Enejder, "Nonlinear microscopy with fiber laser continuum excitation," *J. Biomed. Opt.* **15**(2), 026026 (2010).
34. J. X. Cheng and X. S. Xie, "Coherent anti-Stokes Raman scattering microscopy: instrumentation, theory, and applications," *J. Phys. Chem. B* **108**(3), 827–840 (2004).
35. G. R. Campbell and J. H. Campbell, "Smooth muscle cell phenotypic changes in arterial wall homeostasis: implications for the pathogenesis and atheorsclerosis," *Exp. Mol. Pathol.* **42**(2), 139–162 (1985).